N62 71187

TECHNICAL NOTE

D-913

INVESTIGATION OF THE LOW-SUBSONIC STABILITY AND

CONTROL CHARACTERISTICS OF A FREE-FLYING MODEL OF A

THICK 70° DELTA REENTRY CONFIGURATION

By John W. Paulson and Robert E. Shanks

Langley Research Center
Langley Air Force Base, Va.

NATIONAL AERONAUTICS AND SPACE ADMINISTRATION

WASHINGTON   October 1961

NATIONAL AERONAUTICS AND SPACE ADMINISTRATION

TECHNICAL NOTE D-913

INVESTIGATION OF THE LOW-SUBSONIC STABILITY AND

CONTROL CHARACTERISTICS OF A FREE-FLYING MODEL OF A

THICK 70° DELTA REENTRY CONFIGURATION

By John W. Paulson and Robert E. Shanks

SUMMARY

An investigation of the low-subsonic flight characteristics of a thick 70° delta reentry configuration having a diamond cross section has been made in the Langley full-scale tunnel over an angle-of-attack range from 20° to 45°. Flight tests were also made at angles of attack near maximum lift ($\alpha = 40°$) with a radio-controlled model dropped from a helicopter. Static and dynamic force tests were made over an angle-of-attack range from 0° to 90°.

The longitudinal stability and control characteristics were considered satisfactory when the model had positive static longitudinal stability. It was possible to fly the model with a small amount of static instability, but the longitudinal characteristics were considered unsatisfactory in this condition. At angles of attack above the stall the model developed a large, constant-amplitude pitching oscillation. The lateral stability characteristics were considered to be only fair at angles of attack from about 20° to 35° because of a lightly damped Dutch roll oscillation. At higher angles of attack the oscillation was well damped and the lateral stability was generally satisfactory. The Dutch roll damping at the lower angles of attack was increased to satisfactory values by means of a simple rate-type roll damper. The lateral control characteristics were generally satisfactory throughout the angle-of-attack range, but there was some deterioration in aileron effectiveness in the high angle-of-attack range due mainly to a large increase in damping in roll.

INTRODUCTION

An investigation is being conducted by the National Aeronautics and Space Administration to provide information on the stability and control characteristics of manned space vehicle configurations over the speed range from hypersonic to low subsonic. The present investigation was

made to provide some information at low-subsonic speeds on the longitudinal and lateral stability and control characteristics of a model of a thick 70° delta configuration having a diamond cross section. Static force-test results on the same configuration have been reported in reference 1.

The investigation included flight tests in the Langley full-scale tunnel to determine the low-subsonic flight characteristics of the model over an angle-of-attack range from about 20° to 45°. Flight tests were also made at angles of attack near maximum lift ($\alpha = 40°$) with a radio-controlled model dropped from a helicopter. Force tests were made to determine the static stability and control characteristics and the lateral dynamic stability derivatives from 0° to 90° angle of attack.

SYMBOLS

The longitudinal forces and moments were determined with respect to the wind axes and the lateral forces and moments were determined with respect to the body axes. (See fig. 1.) The axes originated at a center-of-gravity position located at 39 percent mean aerodynamic chord. All measurements are reduced to standard coefficient form and presented in terms of the following symbols:

X,Y,Z body reference axes unless otherwise noted

S wing area, sq ft

b wing span, ft

$\bar{c}$ mean aerodynamic chord, ft

t time

$T_{1/2}$ time to damp to half-amplitude, sec

V free-stream velocity, ft/sec

q free-stream dynamic pressure, lb/sq ft

ω angular velocity, $2\pi f$, radian/sec

f frequency of the oscillation, cps

k reduced frequency parameter, $\omega b/2V$

α	angle of attack, deg
β	angle of sideslip, deg or radians
δ	control deflection, deg
I_X	moment of inertia about longitudinal body axis, slug-ft^2
I_Y	moment of inertia about lateral body axis, slug-ft^2
I_Z	moment of inertia about normal body axis, slug-ft^2
p, q, r	rolling, pitching, and yawing velocity, respectively, radians/sec
$\dot{\beta} = \dfrac{d\beta}{dt}$	
$\dot{r} = \dfrac{dr}{dt}$	
$\dot{p} = \dfrac{dp}{dt}$	
F_L	lift, lb
F_D	drag, lb
F_Y	side force, lb
M_Y	pitching moment, ft-lb
M_X	rolling moment, ft-lb
M_Z	yawing moment, ft-lb
C_L	lift coefficient, F_L/qS
C_D	drag coefficient, F_D/qS
C_Y	side-force coefficient, F_Y/qS
C_m	pitching-moment coefficient, $M_Y/qS\bar{c}$

C_l rolling-moment coefficient, M_X/qSb

C_n yawing-moment coefficient, M_Z/qSb

$$C_{m_\alpha} = \frac{\partial C_m}{\partial \alpha}$$

$$C_{l_\beta} = \frac{\partial C_l}{\partial \beta} \qquad\qquad C_{l_r} = \frac{\partial C_l}{\partial \left(\frac{rb}{2V}\right)} \qquad\qquad C_{l_p} = \frac{\partial C_l}{\partial \left(\frac{pb}{2V}\right)}$$

$$C_{n_\beta} = \frac{\partial C_n}{\partial \beta} \qquad\qquad C_{n_r} = \frac{\partial C_n}{\partial \left(\frac{rb}{2V}\right)} \qquad\qquad C_{n_p} = \frac{\partial C_n}{\partial \left(\frac{pb}{2V}\right)}$$

$$C_{Y_\beta} = \frac{\partial C_Y}{\partial \beta} \qquad\qquad C_{Y_r} = \frac{\partial C_Y}{\partial \left(\frac{rb}{2V}\right)} \qquad\qquad C_{Y_p} = \frac{\partial C_Y}{\partial \left(\frac{pb}{2V}\right)}$$

$$C_{l_{\dot\beta}} = \frac{\partial C_l}{\partial \left(\frac{\dot\beta b}{2V}\right)} \qquad\qquad C_{l_{\dot r}} = \frac{\partial C_l}{\partial \left(\frac{\dot r b^2}{4V^2}\right)} \qquad\qquad C_{l_{\dot p}} = \frac{\partial C_l}{\partial \left(\frac{\dot p b^2}{4V^2}\right)}$$

$$C_{n_{\dot\beta}} = \frac{\partial C_n}{\partial \left(\frac{\dot\beta b}{2V}\right)} \qquad\qquad C_{n_{\dot r}} = \frac{\partial C_n}{\partial \left(\frac{\dot r b^2}{4V^2}\right)} \qquad\qquad C_{n_{\dot p}} = \frac{\partial C_n}{\partial \left(\frac{\dot p b^2}{4V^2}\right)}$$

$$C_{Y_{\dot\beta}} = \frac{\partial C_Y}{\partial \left(\frac{\dot\beta b}{2V}\right)} \qquad\qquad C_{Y_{\dot r}} = \frac{\partial C_Y}{\partial \left(\frac{\dot r b^2}{4V^2}\right)} \qquad\qquad C_{Y_{\dot p}} = \frac{\partial C_Y}{\partial \left(\frac{\dot p b^2}{4V^2}\right)}$$

    The term "in-phase derivative" used herein refers to any one of the stability derivatives which are based on the forces or moments in phase with the angle of roll or yaw produced in the oscillatory tests. The term "out-of-phase derivative" refers to any one of the stability derivatives which are based on the forces or moments 90° out of phase with the angle of roll or yaw. The derivatives were measured in the oscillation tests in the following combinations:

L
1
6
8
4

$$C_{l_\beta} \sin \alpha - k^2 C_{l_{\dot{p}}}$$

$$C_{n_\beta} \sin \alpha - k^2 C_{n_{\dot{p}}}$$ In-phase rolling derivatives

$$C_{Y_\beta} \sin \alpha - k^2 C_{Y_{\dot{p}}}$$

$$C_{l_\beta} \cos \alpha + k^2 C_{l_{\dot{r}}}$$

$$C_{n_\beta} \cos \alpha + k^2 C_{n_{\dot{r}}}$$ In-phase yawing derivatives

$$C_{Y_\beta} \cos \alpha + k^2 C_{Y_{\dot{r}}}$$

$$C_{l_p} + C_{l_{\dot{\beta}}} \sin \alpha$$

$$C_{n_p} + C_{n_{\dot{\beta}}} \sin \alpha$$ Out-of-phase rolling derivatives

$$C_{Y_p} + C_{Y_{\dot{\beta}}} \sin \alpha$$

$$C_{l_r} - C_{l_{\dot{\beta}}} \cos \alpha$$

$$C_{n_r} - C_{n_{\dot{\beta}}} \cos \alpha$$ Out-of-phase yawing derivatives

$$C_{Y_r} - C_{Y_{\dot{\beta}}} \cos \alpha$$

Subscripts:

e   elevator

a   aileron

r   rudder

APPARATUS AND TESTING TECHNIQUE

Model

The model used in the investigation was assumed to be a 1/5-scale
model of a possible manned space vehicle configuration. A three-view
drawing of the model is shown in figure 2, and a photograph of the model
flying in the full-scale tunnel is shown in figure 3. Table I gives the
dimensional and mass characteristics of the model. Elevons consisting
of plain flaps extending rearward from the trailing edge of both the   L
upper and lower surfaces of the wing were deflected together for eleva-   1
tor control and differentially for aileron control, and outward deflec-   6
ting surfaces located at the wing tips were used for rudder control.   8
The model was modified by the addition of a leading-edge transition   4
strip or by the addition of a sharp leading edge. (See fig. 2.)

For the flight tests in the Langley full-scale tunnel, thrust was
provided by compressed air supplied through flexible hoses to a nozzle
at the rear of the fuselage. The controls were operated remotely by
means of electric servomechanisms which gave flicker (full on or off)
controls. Artificial stabilization in roll was provided by a simple
rate damper. An electrically driven gyroscope was the sensing element
and the output signal was fed into a servoactuator which deflected the
elevons in proportion to rolling velocity. The manual control was
superimposed on the control deflection resulting from the rate signal.

For the radio-control tests the model was unpowered. The controls
were operated by means of the same type electric servomechanisms used
in the full-scale tunnel.

Test Equipment and Setup

The static- and rotary-oscillation force tests were conducted at the
Langley Research Center in a low-speed tunnel having a 12-foot octagonal
test section. Detailed descriptions of the oscillation apparatus and
methods used in obtaining and reducing the data are given in reference 2.
The model was sting mounted, and the longitudinal and lateral forces and
moments were measured about the body axes by means of internal strain-
gage balances.

The flight investigation was conducted in the Langley full-scale
tunnel with the test setup illustrated in figure 4. The model was
remotely controlled by a roll-yaw pilot, a pitch pilot, and a thrust
controller. Compressed air for thrust and electric power for the con-
trol actuators was supplied through a slack overhead line which also
acted as a safety cable to prevent the model from crashing when it went

out of control. A more complete description of the tunnel-test technique used in making free-flying model tests is given in reference 3.

In the radio-control tests the unpowered model was dropped from a helicopter and controlled during the gliding flight by two ground located pilots, one of whom handled the lateral control and the other the pitch control. The model was landed by a parachute. A more complete description of the radio-control technique is given in reference 4.

STABILITY AND CONTROL PARAMETERS OF FLIGHT-TEST MODEL

Force tests were made to determine the static longitudinal and lateral stability and control characteristics of the model. The tests were made at a dynamic pressure of 4 pounds per square foot which corresponds to an airspeed of 58 feet per second at standard sea-level conditions and to a test Reynolds number of 1,340,000 based on the mean aerodynamic chord of 3.61 feet.

Static Longitudinal Stability and Control

The static longitudinal stability and control tests were made for an angle-of-attack range from $0°$ to $90°$ for elevator settings from $5°$ to $-15°$ in $5°$ increments. These data are presented in figure 5 and show that the model was about neutrally stable up to the stall and stable beyond the stall. The pitching moment produced by elevator deflection was generally fairly constant up to the stall, but decreased somewhat at higher angles of attack.

Since the leading-edge radius was fairly large for the basic configuration in order to reduce the heating problems at hypersonic speeds, a few tests were made with a very sharp leading edge (fig. 2) to see if there was an appreciable effect of leading-edge shape on the low-speed characteristics. Tests were also made with a transition strip similar to that studied in reference 1 to simulate higher Reynolds number data by insuring turbulent flow behind the transition strip. Presented in figure 6 is a comparison of the longitudinal characteristics of the basic model with those of the model with the transition strip and with the sharp leading edge for a center-of-gravity position of $0.39\bar{c}$ for each configuration. The data show that the transition strip did not greatly alter the characteristics of the basic model indicating that the low-scale data were generally representative of higher-scale data. The addition of the sharp leading edge resulted in a large increase in lift-curve slope and also caused the model to become longitudinally unstable.

Static Lateral Stability and Control

The static lateral stability tests were made over a range of sideslip angles from 20° to -20° for angles of attack from 0° to 90°. The data are presented as the variation of the coefficients C_Y, C_n, and C_l with angle of sideslip for various angles of attack in figure 7 for the basic model and for the model with the transition strip and with the sharp leading edge. These data are summarized in figure 8 as the variation with angle of attack of the side-force parameter C_{Y_β}, the directional-stability parameter C_{n_β}, and the effective-dihedral parameter $-C_{l_\beta}$ which were obtained by taking the difference between the values of the coefficients measured at angles of sideslip between -5° and 5°. The data of figure 8 show that all three configurations had about the same amount of directional stability up to about 25° angle of attack but there were large differences in the directional stability characteristics at the higher angles of attack. The model had positive effective dihedral over the angle-of-attack range for all conditions.

The rudder and aileron characteristics from 0° to 90° angle of attack are presented in figure 9. The data show that yawing moments produced by the rudder increased up to about 20° angle of attack and then gradually decreased as the angle of attack increased. The aileron effectiveness decreased with increasing angle of attack and became rather low at angles of attack above about 50°. The yawing moment produced by the aileron was about zero or positive, depending on the elevator setting, up to about 40° angle of attack and then became very adverse at higher angles of attack.

Dynamic Stability Derivatives

The variation of the out-of-phase rolling and yawing derivatives with angle of attack for the basic model are presented in figure 10, for values of the reduced frequency parameter k of 0.10, 0.15, and 0.20. The data show that the damping-in-roll parameter $C_{l_p} + C_{l_{\dot\beta}} \sin \alpha$ was negative (indicating positive damping) over the angle-of-attack range and had the highest value at an angle of attack near 50°. The damping-in-yaw parameter $C_{n_r} - C_{n_{\dot\beta}} \cos \alpha$ was negative (positive damping) in the low angle-of-attack range but became unstable from 20° to 50° angle of attack, depending on the frequency. The greatest effects of frequency usually occurred above 20° or 30° angle of attack. The comparison of the out-of-phase derivatives for the basic model and for the model with the transition strip at one frequency ($k = 0.15$) presented in figure 11 shows that, in general, the transition strip did not greatly affect the derivatives.

The in-phase rolling and yawing derivatives for the basic model
are presented in figure 12 and generally show little effect of fre-
quency. A comparison is made in figure 13 between the in-phase deriva-
tives for the basic model and for the model with the transition strip
at one frequency (k = 0.15). These data show that there was very little
difference in the characteristics of the two configurations.

<div align="center">CALCULATIONS</div>

Calculations were made to determine the period and time to damp
to half-amplitude of the Dutch roll oscillation of the basic model over
the angle-of-attack range from 5° to 40°. Calculations were also made
at 20° and 35° angle of attack to determine the effect of variations in
the derivatives C_{l_p}, C_{n_r}, and C_{n_p} on the time to damp to half-
amplitude of the oscillation. The calculations were made using the
equations of reference 5 except that they were referred to the body
axes. The derivatives measured in the force-test investigation were
used in making the calculations.

Presented in figure 14 is the variation with angle of attack of the
period and the reciprocal of the time to damp to half-amplitude. These
data show that the oscillation was well damped at low and high angles
of attack but was only lightly damped at angles of attack near 20°.
There was very little change in period over most of the angle-of-attack
range.

Presented in figure 15 is the effect on the time to damp to half-
amplitude of variations in the derivatives C_{l_p}, C_{n_p}, and C_{n_r} at
angles of attack of 20° and 35°. It is seen that C_{l_p} had a large
effect on the damping of the oscillation at both angles of attack while
changes in C_{n_r} had little effect. It is of interest to note that
C_{n_p} had a large effect on the damping particularly at 20° angle of
attack where two oscillatory modes appeared when C_{n_p} increased above
about 0.1. As C_{n_p} was increased further, one mode became more stable
while the other became unstable. It should be pointed out here that
in cases where the ailerons used for roll damping produce large yawing
moments the effect of C_{n_p} can be significant. In such cases the
damper will produce C_{n_p} as well as C_{l_p}, and the C_{n_p} contribution
will be stabilizing when the aileron yawing moments are adverse and
destabilizing when they are favorable.

FLIGHT TESTS

Flight tests were made to determine the dynamic stability and control characteristics of the model over an angle-of-attack range from about $20°$ to $45°$. Flights were made at an angle of attack of $20°$ to determine the effect of center-of-gravity position on the longitudinal characteristics of the model. Flights were also made over the angle-of-attack range to determine the effect of artificial roll damping on the lateral stability and control characteristics. A few flights were made with the transition strip to simulate higher Reynolds numbers but no flights were made with the sharp leading edge.

Coordinated aileron and rudder control was used for most of the tests although some flights were made with ailerons alone. The control deflections used for most of the flights were $\delta_a = \pm 8°$ (each surface), $\delta_e = \pm 5°$, and $\delta_r = \pm 10°$ (one surface).

The model behavior during flight was observed by the pitch pilot located at the side of the test section and by the roll-yaw pilot located in the rear of the test section. The results obtained in the flight tests were primarily in the form of qualitative ratings of flight behavior based on pilot opinion. The motion-picture records obtained in the tests were used to verify and correlate the ratings for the different flight conditions.

FLIGHT-TEST RESULTS AND DISCUSSION

A motion-picture film supplement covering flight tests of the model has been prepared and is available on loan. A request card form and a description of the film will be found at the back of this paper on the page immediately preceding the abstract and index page.

In the following discussion all the results presented will be for the low-scale basic model, but the results are felt to be generally applicable to higher Reynolds number conditions since the results of a few flights made with the transition strips on to simulate a high Reynolds number condition were in close agreement with results obtained in the tests of the basic model.

Longitudinal Stability and Control

During the investigation made to study the longitudinal stability and control characteristics of the model, artificial damping in roll

was used in order to minimize any effects lateral motions might have on the longitudinal behavior.

As part of the longitudinal investigation a series of flights were made at 20° angle of attack to determine the effect of center-of-gravity location. Static tests indicated that at this angle of attack the model was neutrally stable with the center of gravity at about 39 percent of the mean aerodynamic chord. With positive static longitudinal stability (center of gravity ahead of the 39-percent mean-aerodynamic-chord location) the model was easy to fly and the pilot had no trouble controlling it. With neutral stability the model was somewhat more difficult to fly in that it required more attention on the part of the pilot to keep it flying smoothly. With the center of gravity at 42 percent of the mean aerodynamic chord the model was definitely unstable and reacted rather sharply to gusts and control disturbances, but it could be flown fairly easily if the pilot paid very close attention to elevator control. With the center of gravity at 43 percent of the mean aerodynamic chord the model was more sensitive to disturbances but could be flown with constant attention to the elevator control. This was considered the most rearward center-of-gravity position at which sustained flights could be made. A few flights were attempted with the center of gravity at 44 percent of the mean aerodynamic chord; but as soon as the model was disturbed, it diverged rapidly in pitch. Previous investigations (for example, ref. 3) have indicated that the most rearward center-of-gravity position for which flights were possible corresponded approximately to the maneuver point. On the basis of these results, it appears that for this model the maneuver point is about 4 percent aft of the aerodynamic center which seems to be reasonable for this configuration.

In addition to the center-of-gravity range studies made at an angle of attack of 20°, flights were made at angles of attack from about 20° to 45° with a center-of-gravity location $(0.36\bar{c})$ that gave good static longitudinal stability at an angle of attack of 20°. The longitudinal characteristics of the model were generally satisfactory over the entire angle-of-attack range of the investigation.

Lateral Stability and Control

At the lowest angle of attack flown (20°), the model had a lightly damped Dutch roll oscillation (see fig. 14); but it was not particularly troublesome and could be easily controlled by proper use of the ailerons and rudders. Artificial roll damping was effective in stabilizing the oscillation. As the angle of attack increased, the damping of the Dutch roll oscillation also increased until at angles of attack above about 35° the motions of the model were well damped without the roll damper and the model flew very smoothly. These flight-test results are in

agreement with the calculated Dutch roll oscillation characteristics shown in figure 14.

The lateral control characteristics of the model were considered to be generally satisfactory for the angle-of-attack range flown when coordinated aileron and rudder control was used. There appeared to be a deterioration in control effectiveness at the higher angles of attack, but satisfactory control of the model could be maintained. The data of figure 9 show that above 20° angle of attack there was a large decrease in aileron effectiveness for a given elevator setting. However, since up-elevator deflection increased the aileron effectiveness there actually was only a small change in control over the angle-of-attack range flown because of the up elevator required for trim as the angle of attack increased. The main reason for the reduction in controllability at the higher angles of attack was probably the large increase in damping in roll (see fig. 10). It was possible to make satisfactory flights with ailerons alone used for roll control as long as the model was not greatly disturbed. If the model experienced a sizable lateral disturbance, however, it became extremely difficult to stop the resulting motions.

Radio-Control Tests

A few flights were made with the radio-controlled model to check the stability and control characteristics at angles of attack near the stall. The results of these tests were generally in agreement with those found in the Langley full-scale tunnel flight tests. Records from two of the flights are presented in figure 16. In figure 16(a) it is seen that after an initial down-elevator deflection, to insure that the model would clear the helicopter, the elevator was returned to neutral $\left(\delta_e = -5°\right)$ and the model trimmed at an angle of attack of 40° or 50°. A comparison of the time history of the bank angle with the application of the coordinated aileron and rudder control shows that the model responded fairly well to control. In the second flight (fig. 16(b)), when an effort was made to trim at a higher angle of attack, the model developed a large constant-amplitude pitching motion which resulted in angle-of-attack changes from 20° to 80°. There was no large rolling motion associated with this pitching motion, and lateral control was used only in an effort to maintain a particular heading. Subsequent flights showed that the pitching motion could be stopped by using a down elevator to trim the model at a lower angle of attack. The large constant-amplitude pitching motion can probably be attributed to very low or negative values of damping in pitch and to large values of $-C_{m_\alpha}$ at the higher angles of attack.

CONCLUSIONS

The results of the investigation may be summarized as follows:

1. The longitudinal stability and control characteristics of the model were satisfactory when the model had positive static longitudinal stability. It was possible to fly the model with a small amount of static instability, but the longitudinal characteristics were considered unsatisfactory in this condition.

2. At angles of attack above the stall the model developed a large, constant-amplitude pitching oscillation.

3. The lateral stability characteristics were considered to be only fair in the angle-of-attack range from 20° to 35° because of a lightly damped Dutch roll oscillation. Artificial roll damping was effective in stabilizing the Dutch roll oscillation. At higher angles of attack the oscillation was well damped without the roll damper and the lateral stability was satisfactory.

4. The lateral control characteristics were generally satisfactory throughout the angle-of-attack range, but there was some deterioration in aileron effectiveness in the high angle-of-attack range due mainly to a large increase in damping in roll.

Langley Research Center,
    National Aeronautics and Space Administration,
        Langley Air Force Base, Va., July 25, 1961.

14

REFERENCES

1. Paulson, John W.: Low-Speed Static Stability Characteristics of Two
   Configurations Suitable for Lifting Reentry From Satellite Orbit.
   NASA MEMO 10-22-58L, 1958.

2. Hewes, Donald E.: Low-Subsonic Measurements of the Static and Oscil-
   latory Lateral Stability Derivatives of a Sweptback-Wing Airplane
   Configuration at Angles of Attack From -10° to 90°. NASA
   MEMO 5-20-59L, 1959.

3. Paulson, John W., and Shanks, Robert E.: Investigation of Low-Subsonic
   Flight Characteristics of a Model of a Hypersonic Boost-Glide Con-
   figuration Having a 78° Delta Wing. NASA TN D-894, 1961. (Super-
   sedes NASA TM X-201.)

4. Hewes, Donald E., and Hassell, James L., Jr.: Subsonic Flight Tests
   of a 1/7-Scale Radio-Controlled Model of the North American
   X-15 Airplane With Particular Reference to High Angle-of-Attack
   Conditions. NASA TM X-283, 1960.

5. Campbell, John P., and Woodling, Carroll H.: Calculated Effects of
   the Lateral Acceleration Derivatives on the Dynamic Lateral Sta-
   bility of a Delta-Wing Airplane. NACA RM L54K26, 1955.

L
1
6
8
4

TABLE I

DIMENSIONAL AND MASS CHARACTERISTICS OF THE MODEL

Gross weight, lb 41

I_X, slug-ft^2 . . . . 0.55

I_Y, slug-ft^2 . . . . 1.80

I_Z, slug-ft^2 . . . . 2.35

Airfoil section . . . . Wedge

Area (includes cutouts between control surfaces), sq ft 9.73

Span, ft 3.21

Aspect ratio 1.06

Root chord, ft 5.18

Tip chord, ft 0

Mean aerodynamic chord, ft 3.61

Sweepback of leading edge, deg 70

Dihedral 0
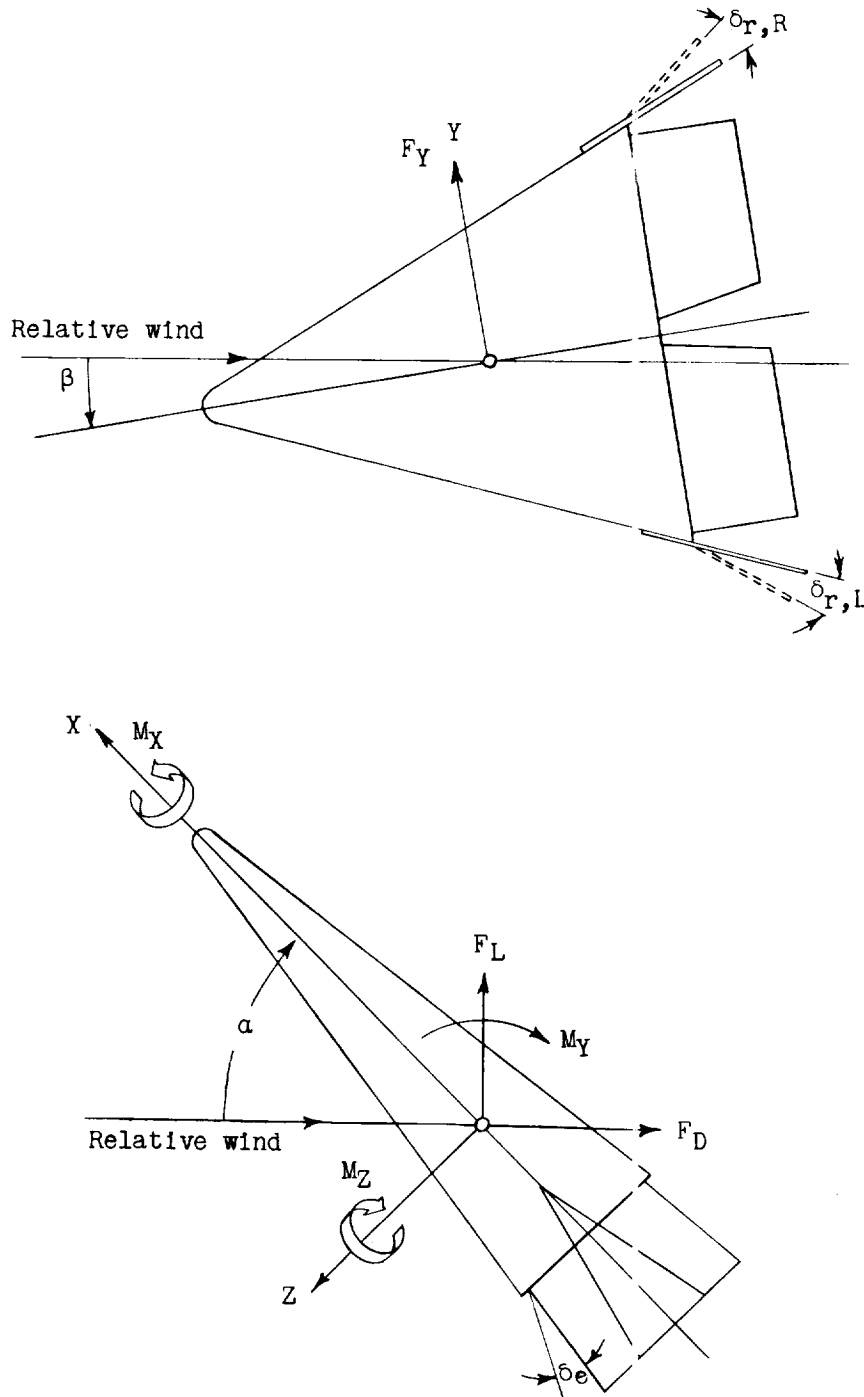
Figure 1.- Sketch of body-axis system showing positive direction of forces, moments, and angles.

Section A — A

Constant 1.5 Rad

15.5

16.7

3.0

A   A

20°

1.5 Rad.

Sharp leading edge

1.0

9.0

14.0

.125 Diam. transition strip

38.5

9.9   50.6   11.5

1.5 Rad.

7.5°

8.2

18.2
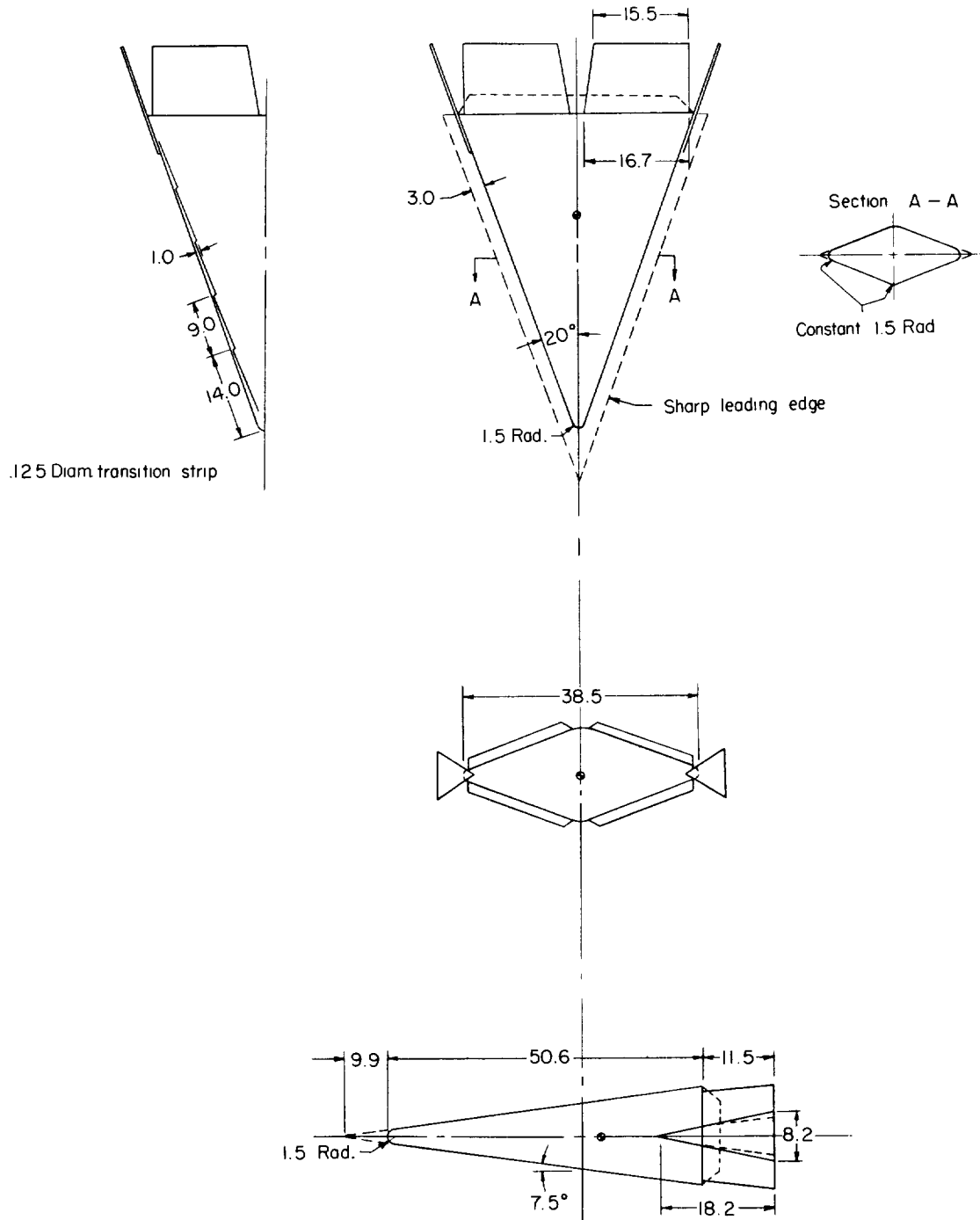
Figure 2.- Three-view drawing of models used in investigation.
All dimensions are in inches.
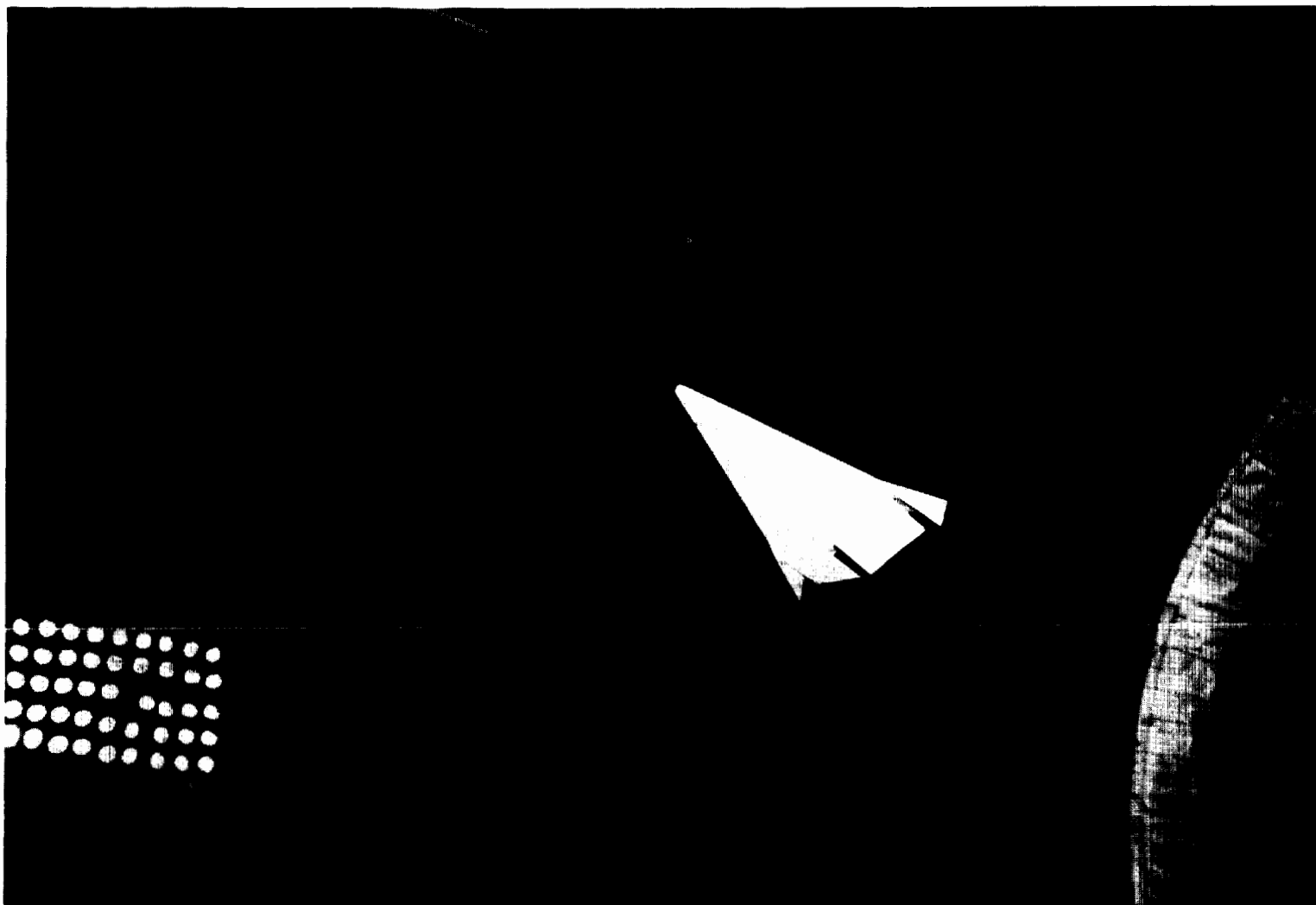
Figure 3.- Model flying in Langley full-scale tunnel.   L-59-2147
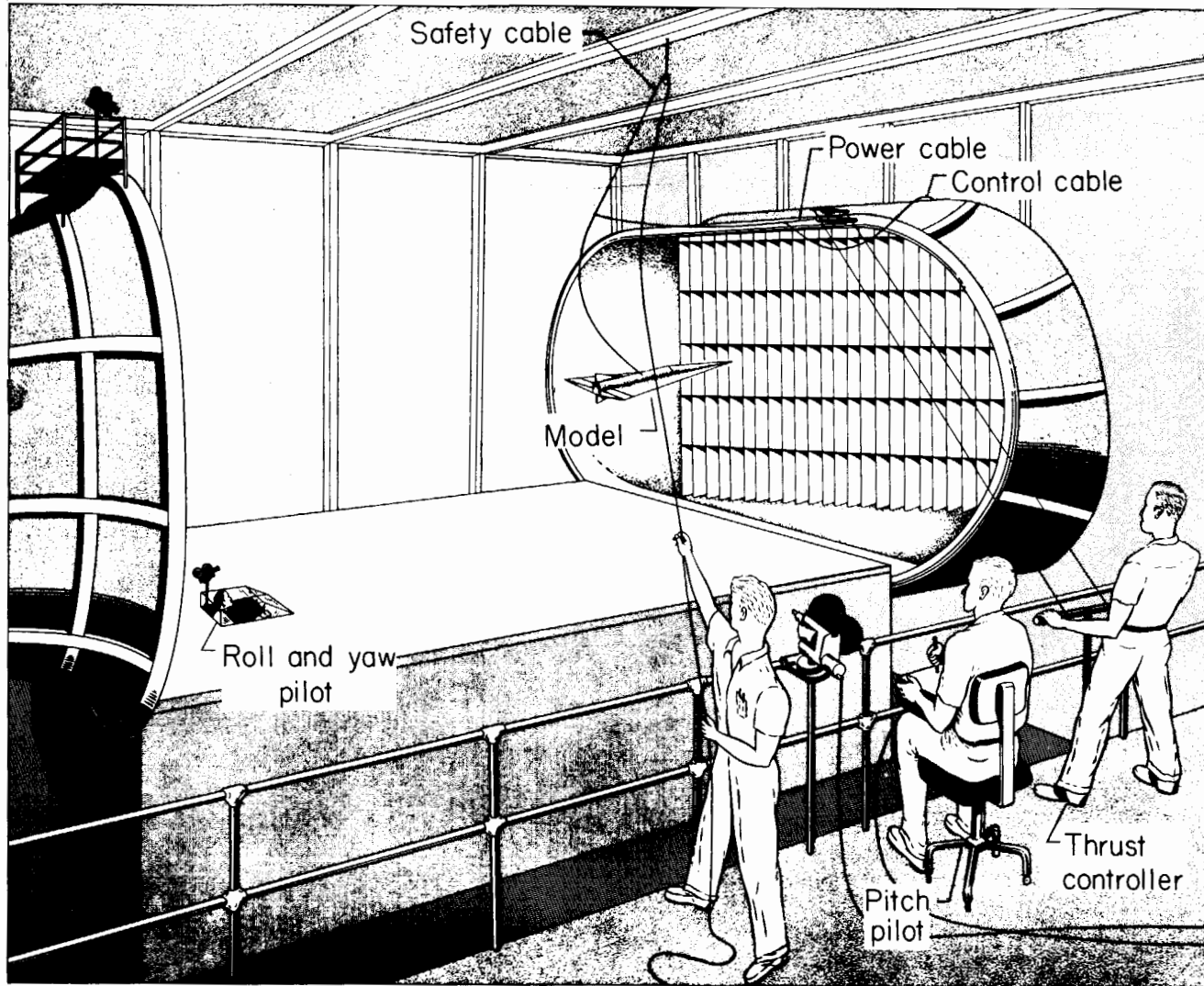
Figure 4.- Flight-test setup in Langley full-scale tunnel.
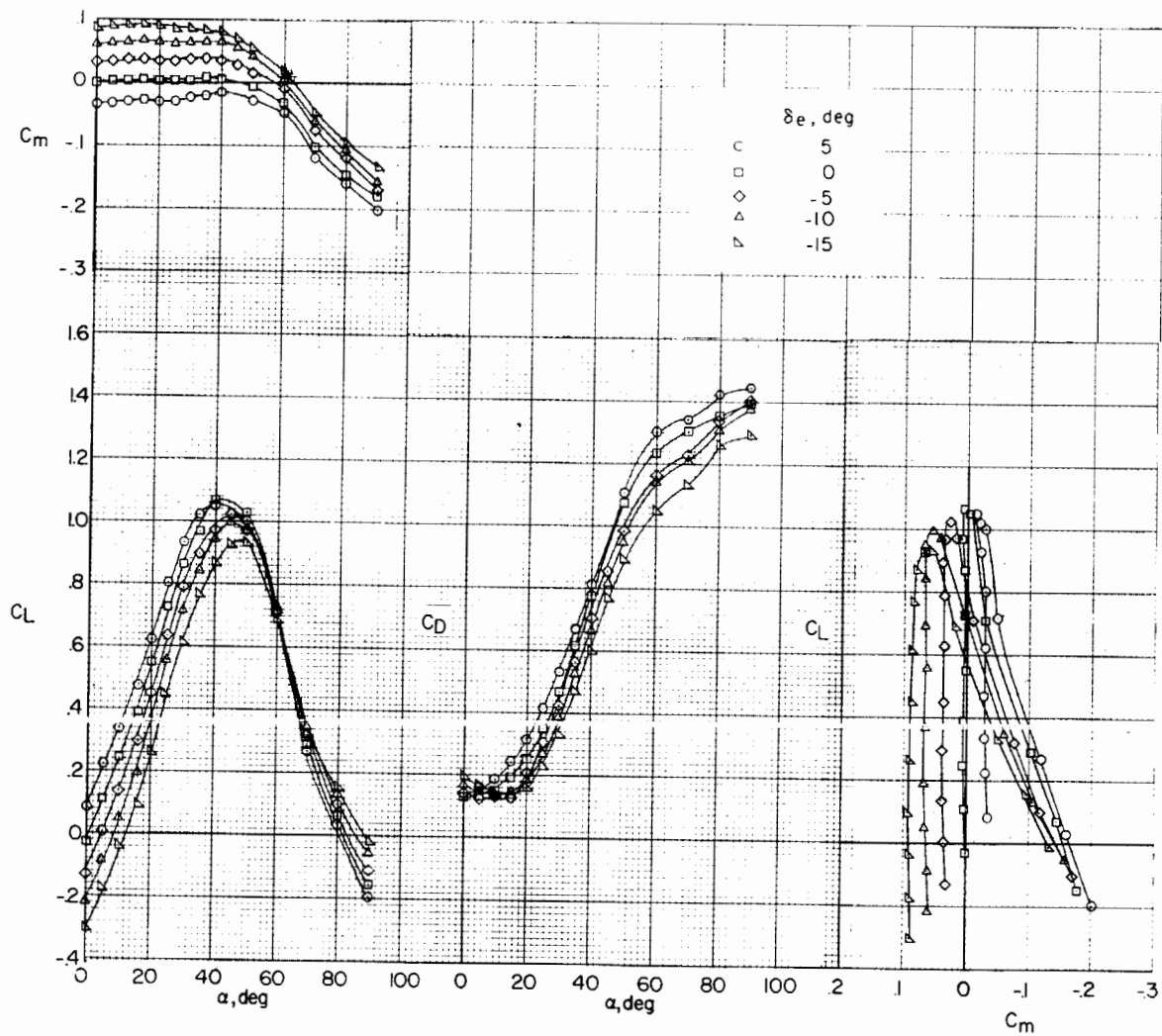
Figure 5.- Effect of elevator deflection on the longitudinal characteristics of the basic model. $\beta = 0^\circ$.

L-1684
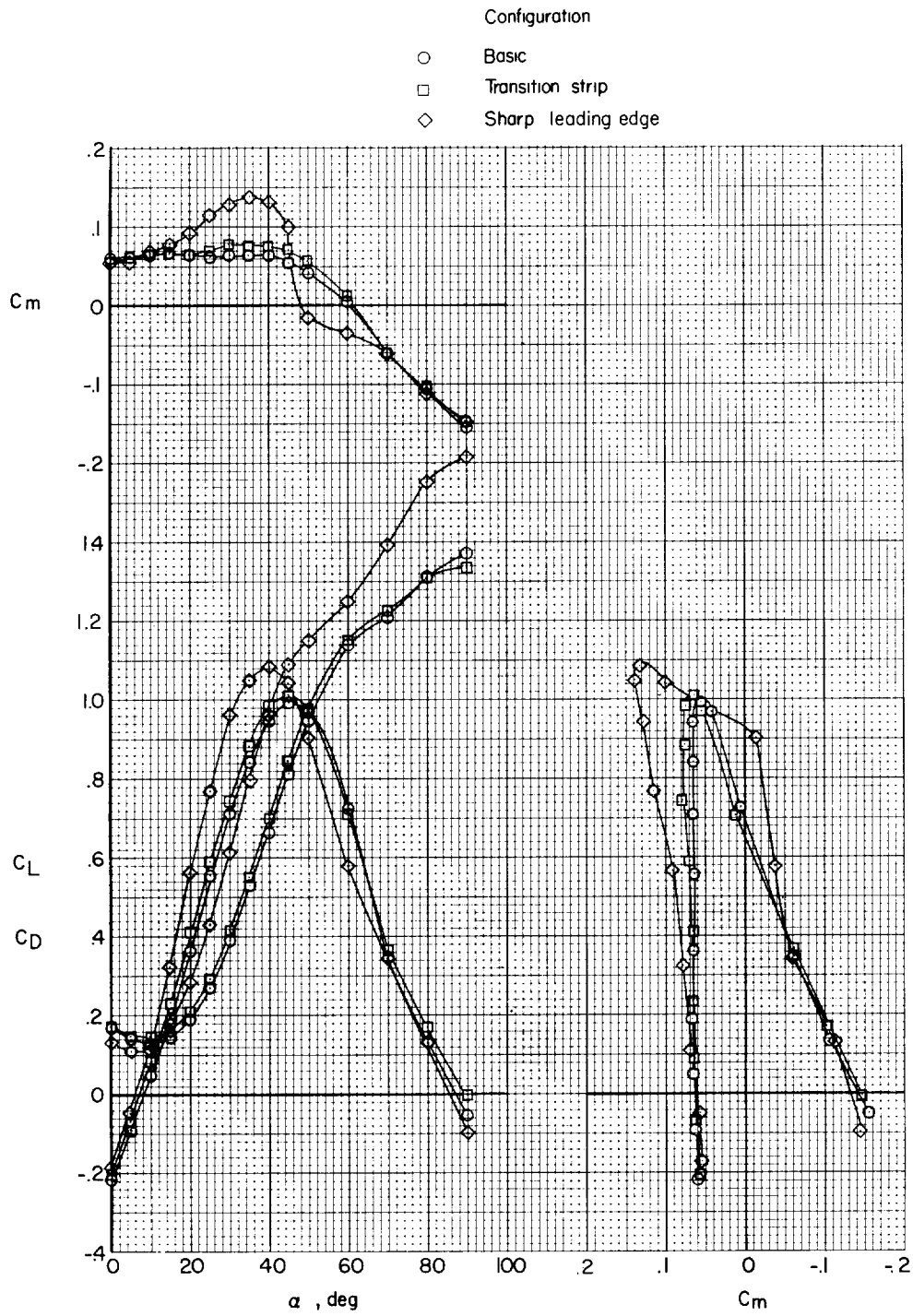
Figure 6.- Effect of leading-edge modification on the longitudinal
characteristics. $\beta = 0^\circ$.

	α, deg			α, deg
○	0		▽	45
□	10		◻	50
◇	20		◊	55
△	25		◊	60
◣	30		△	70
◹	40		▽	80
			▽	90
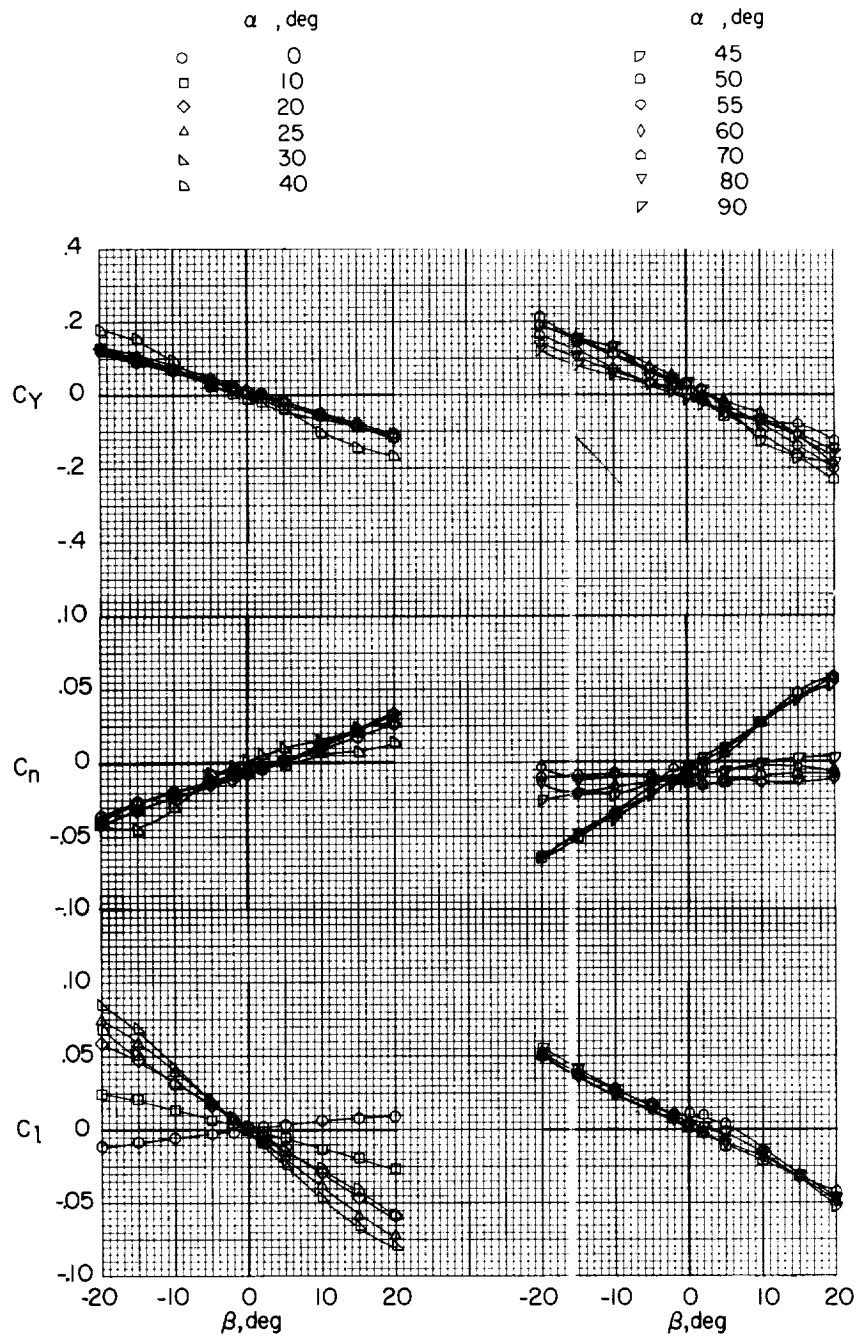
(a) Basic; $\delta_e = -10^\circ$.

Figure 7.- Variation of static lateral stability coefficients with angle of sideslip.

	α ,deg		α ,deg
○	0	◻	50
◻	10	◇	55
◇	20	◇	60
△	25	△	70
△	30	▽	80
◻	40	▷	90
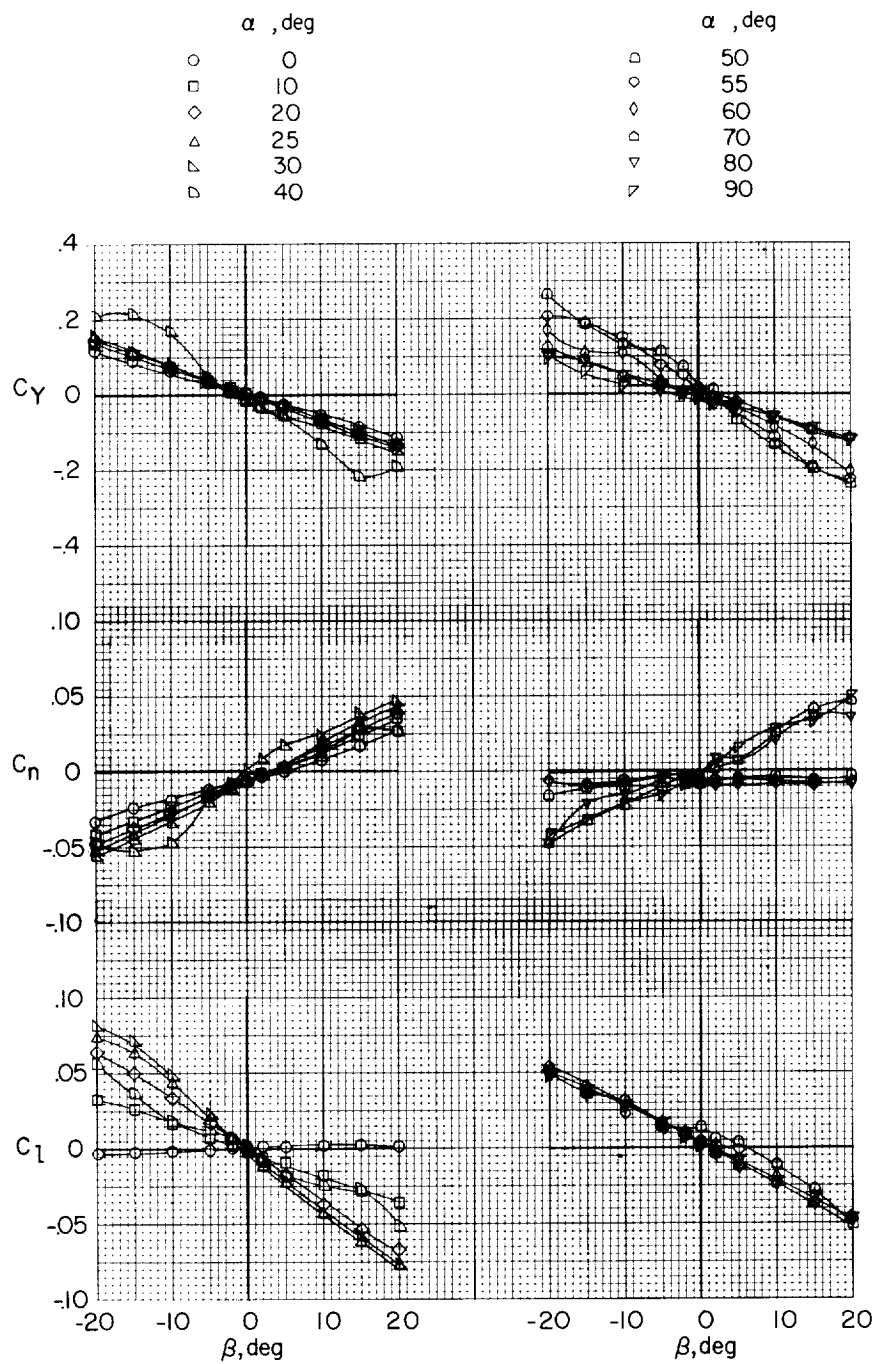
(b) Transition strip; $\delta_e = 0°$.

Figure 7.- Continued.

	α , deg			α , deg
○	0		◻	50
◇	20		○	55
◁	30		◇	60
◻	40		△	70
			▽	80
			▷	90
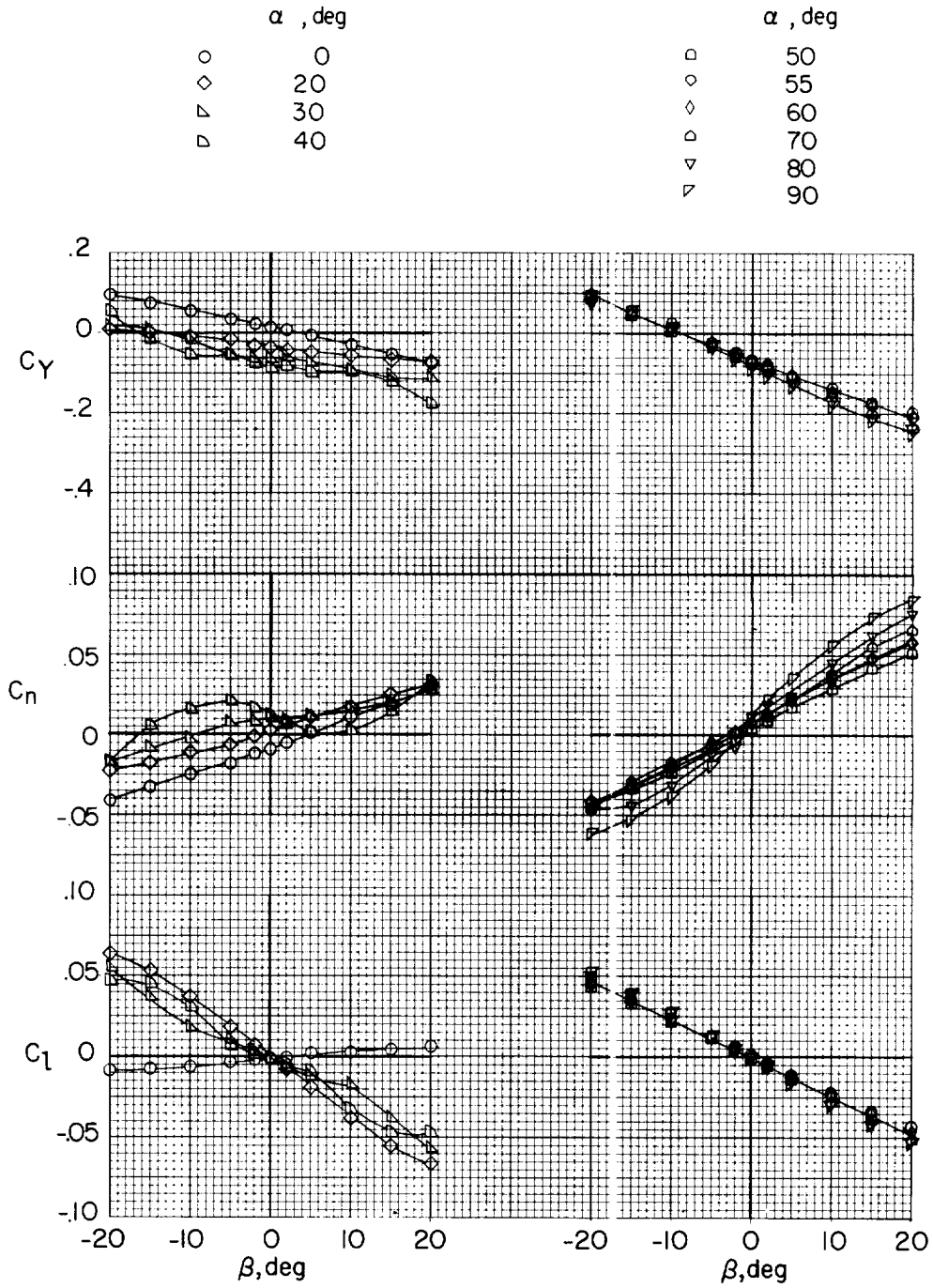
(c) Sharp leading edge; $\delta_e = 0°$.

Figure 7.- Concluded.

L-1684
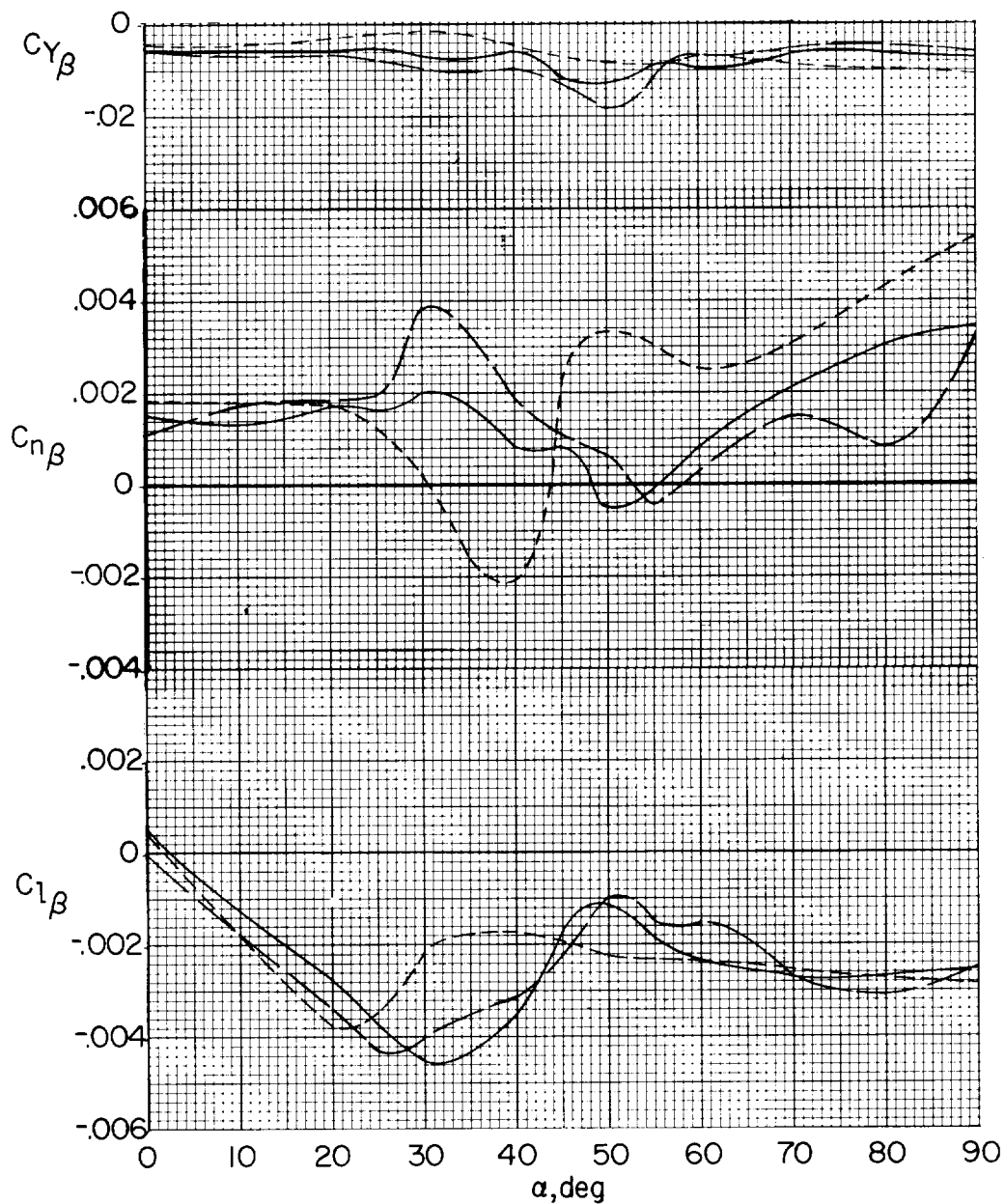
Figure 8.- Variation of the static lateral stability derivatives with angle of attack. $\beta = -5^\circ$ to 5°.
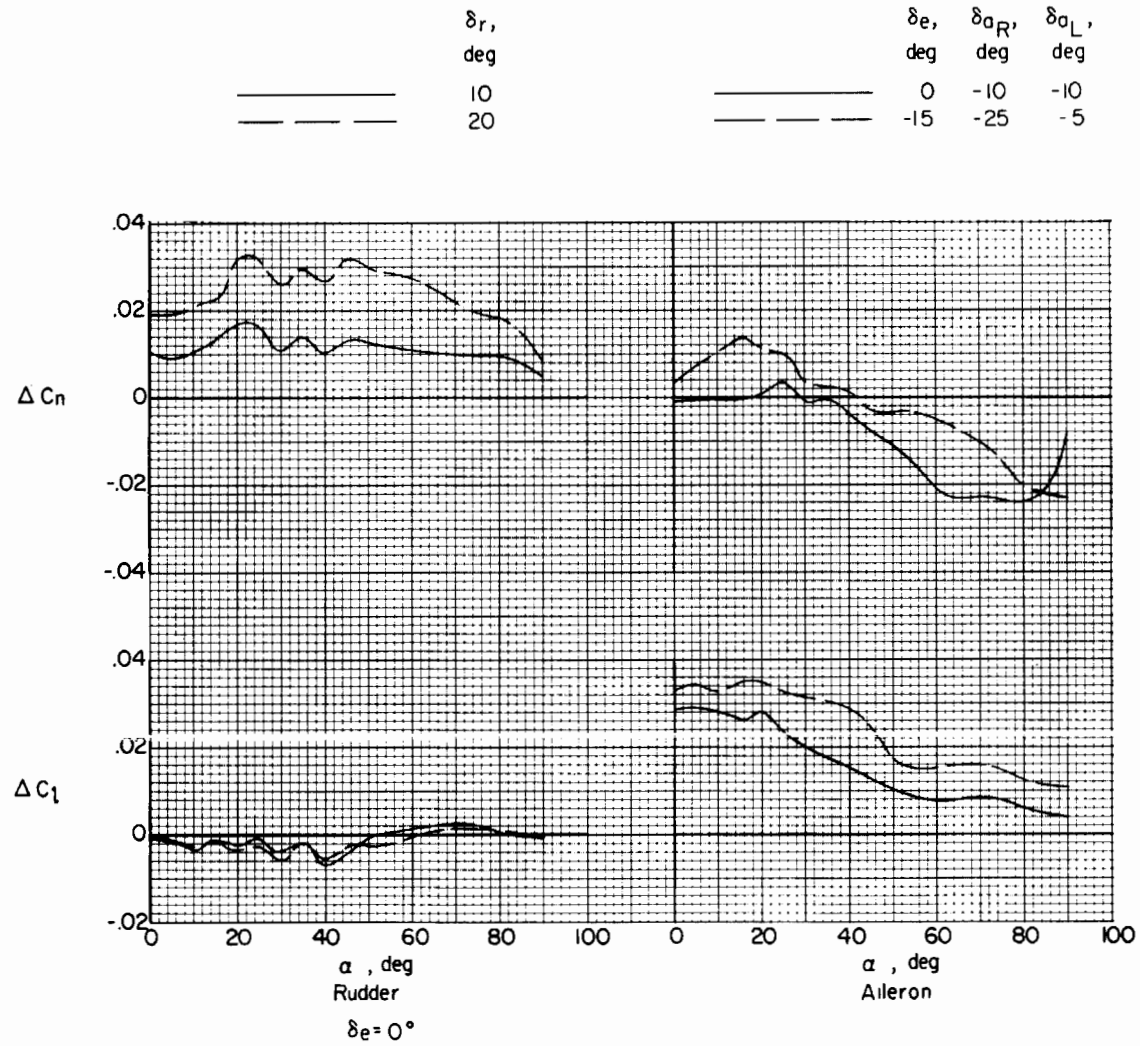
Figure 9.- Incremental lateral control coefficients for rudder and aileron characteristics. β = 0°.
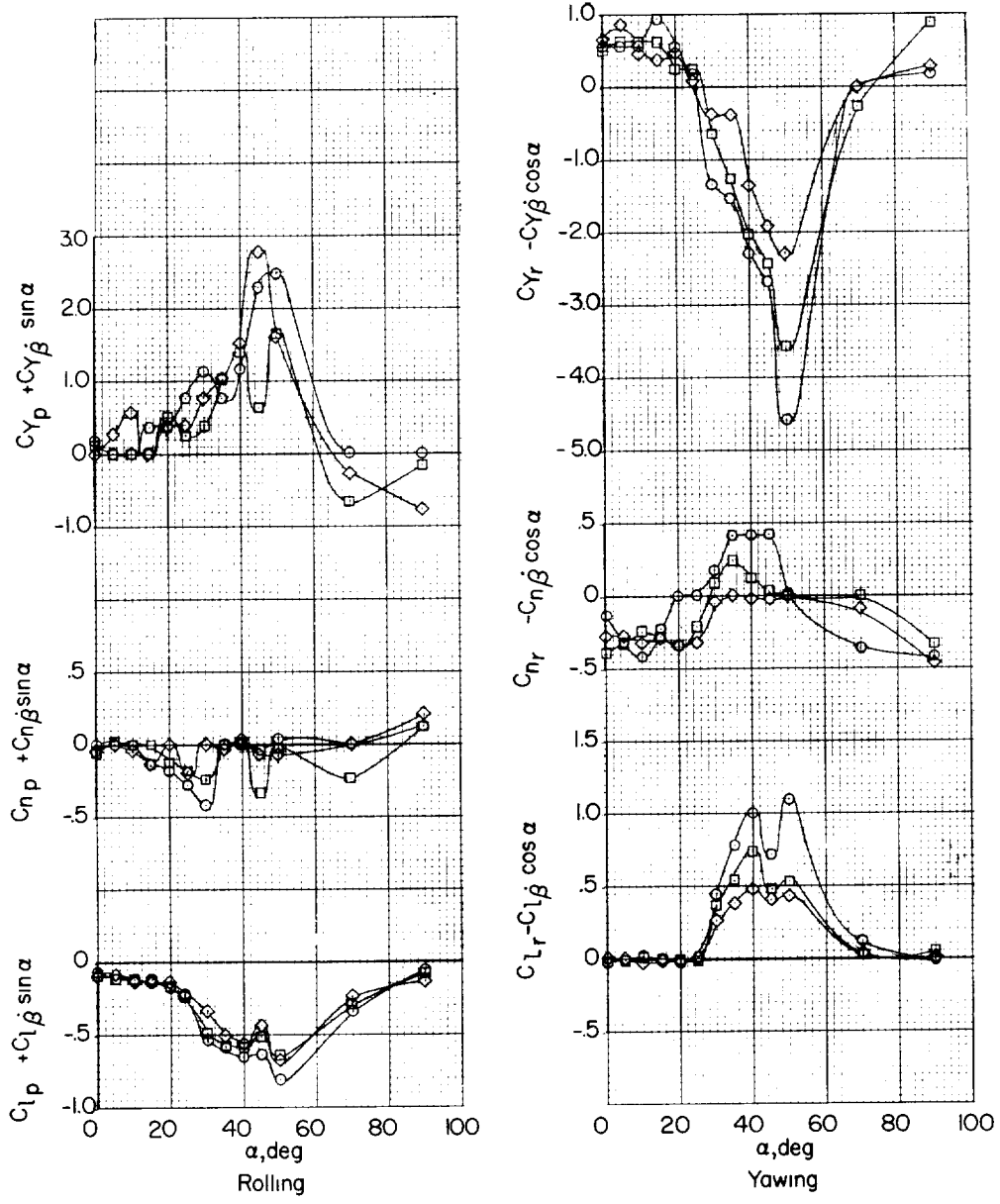
Figure 10.- Variation of the out-of-phase rolling and yawing derivatives with angle of attack for the basic model.
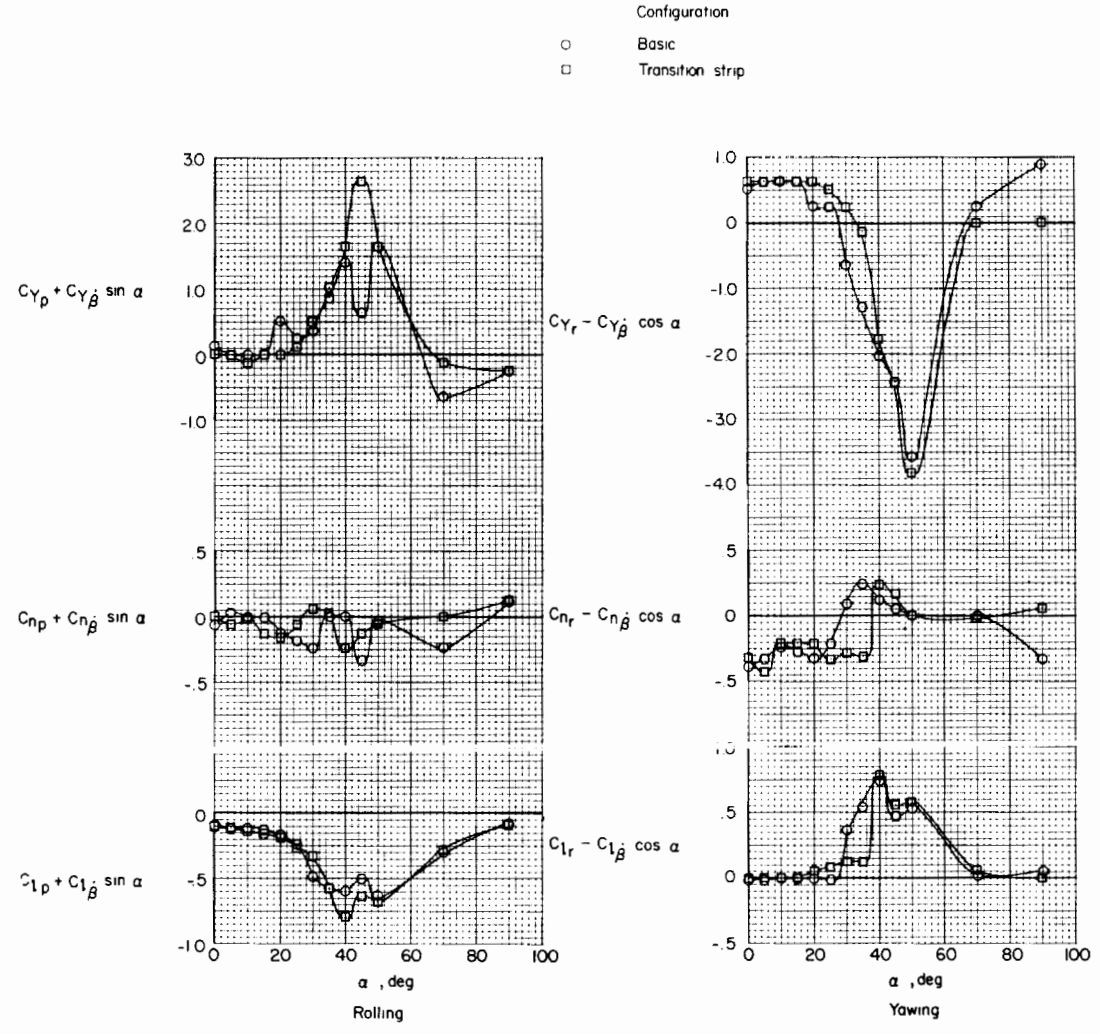
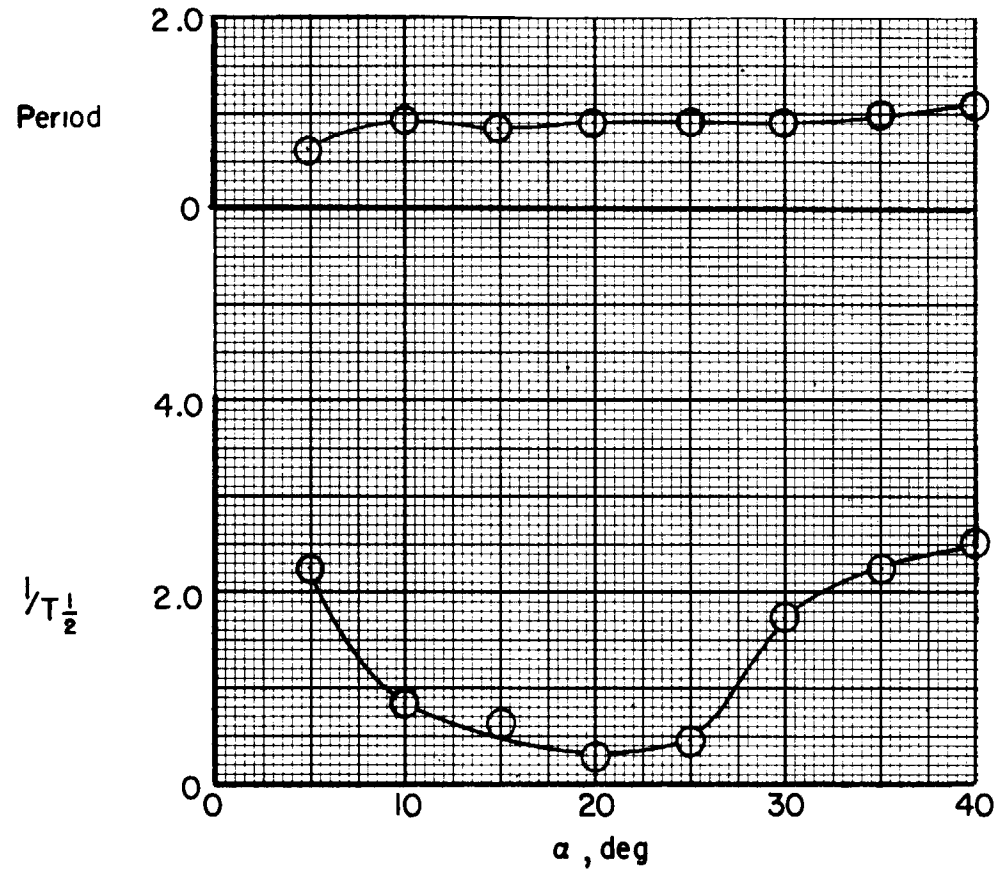Figure 11.- Effect of leading-edge modification on the out-of-phase rolling and yawing derivatives. k = 0.15.
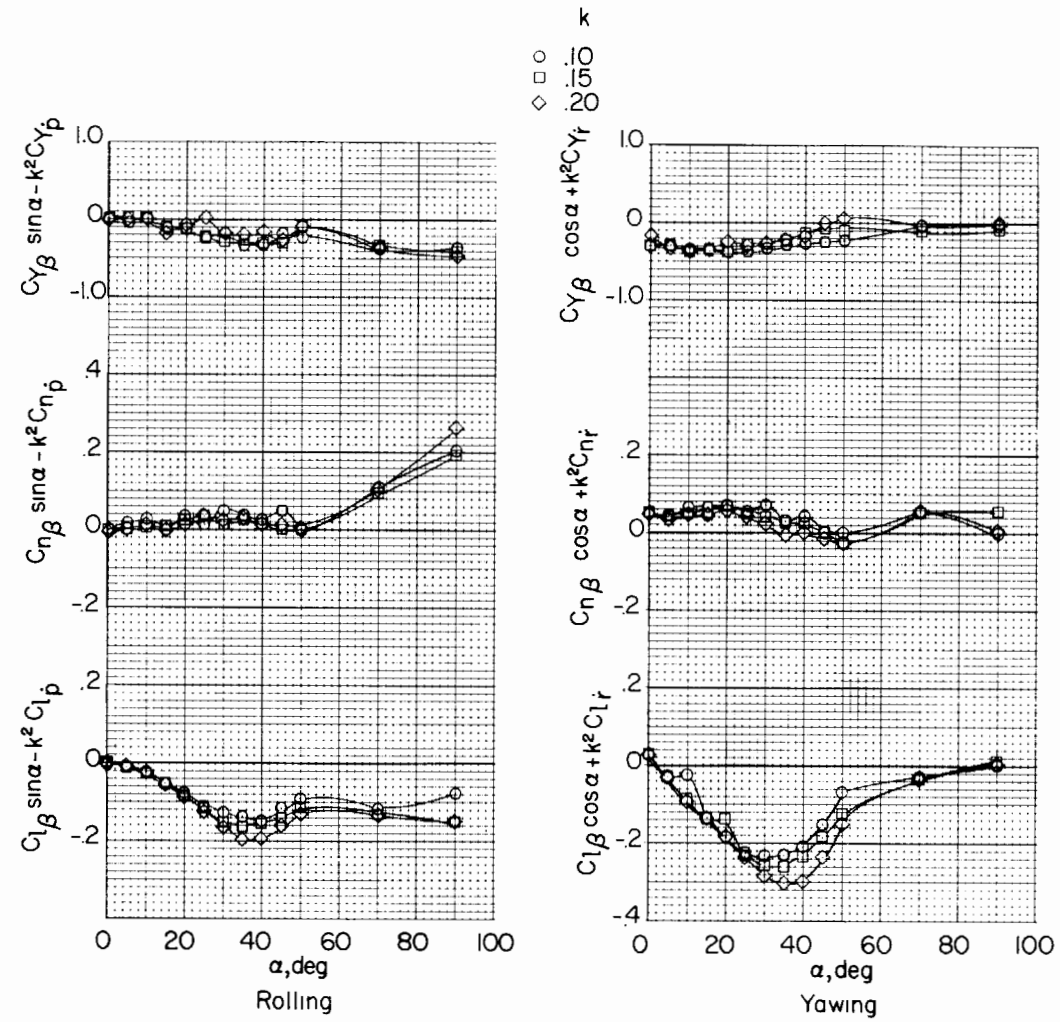
Figure 12.- Variation of in-phase rolling and yawing derivatives with angle of attack for the basic model.
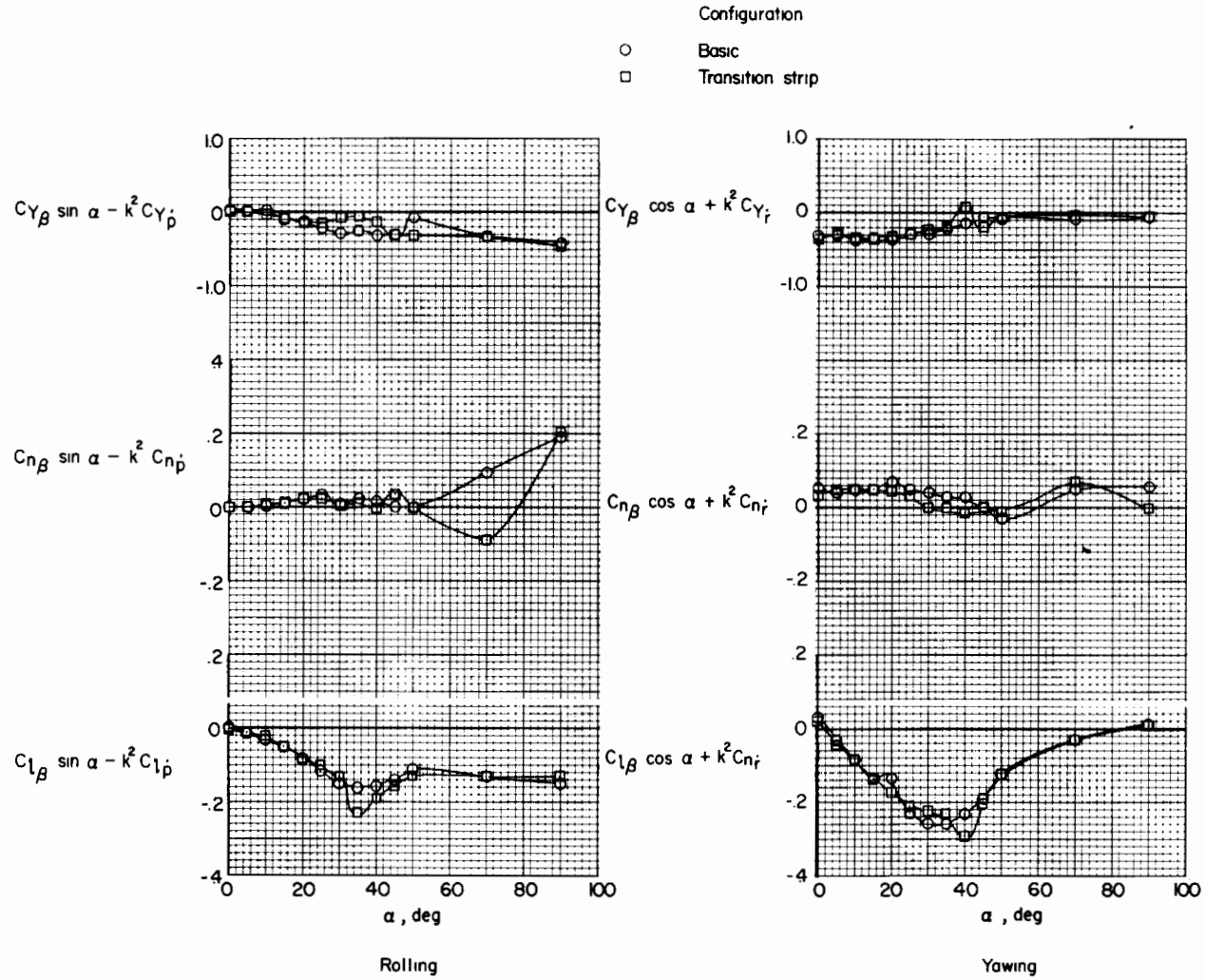
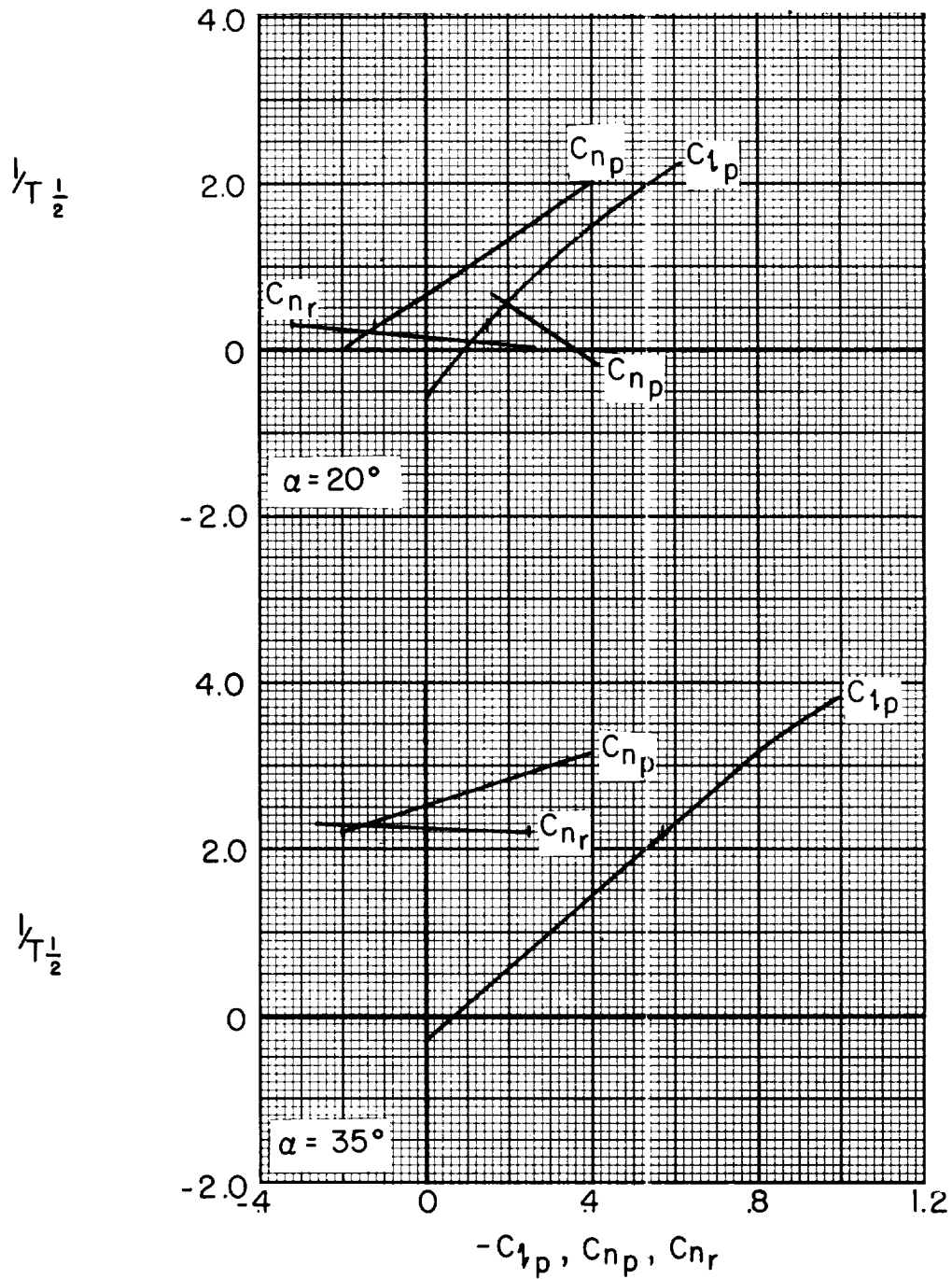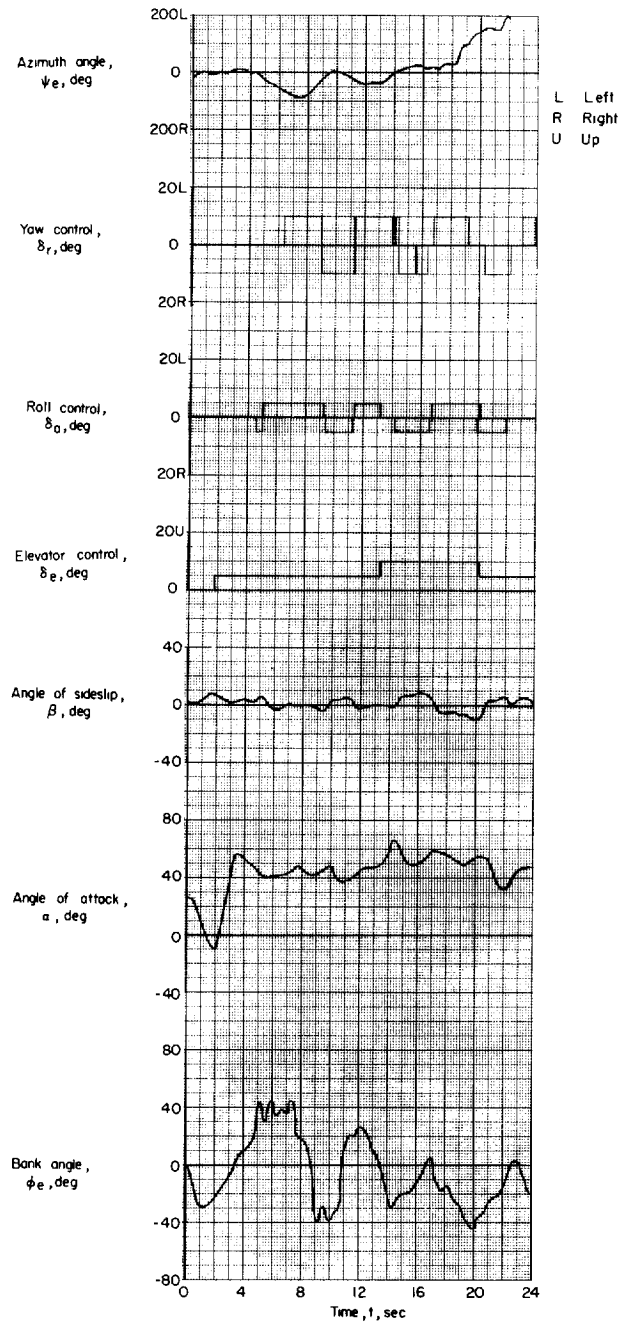Figure 13.- Effect of leading-edge modification on the in-phase rolling and yawing derivatives. k = 0.15.

Figure 14.- Calculated period and time to damp to half-amplitude of the Dutch roll oscillation for the basic model.
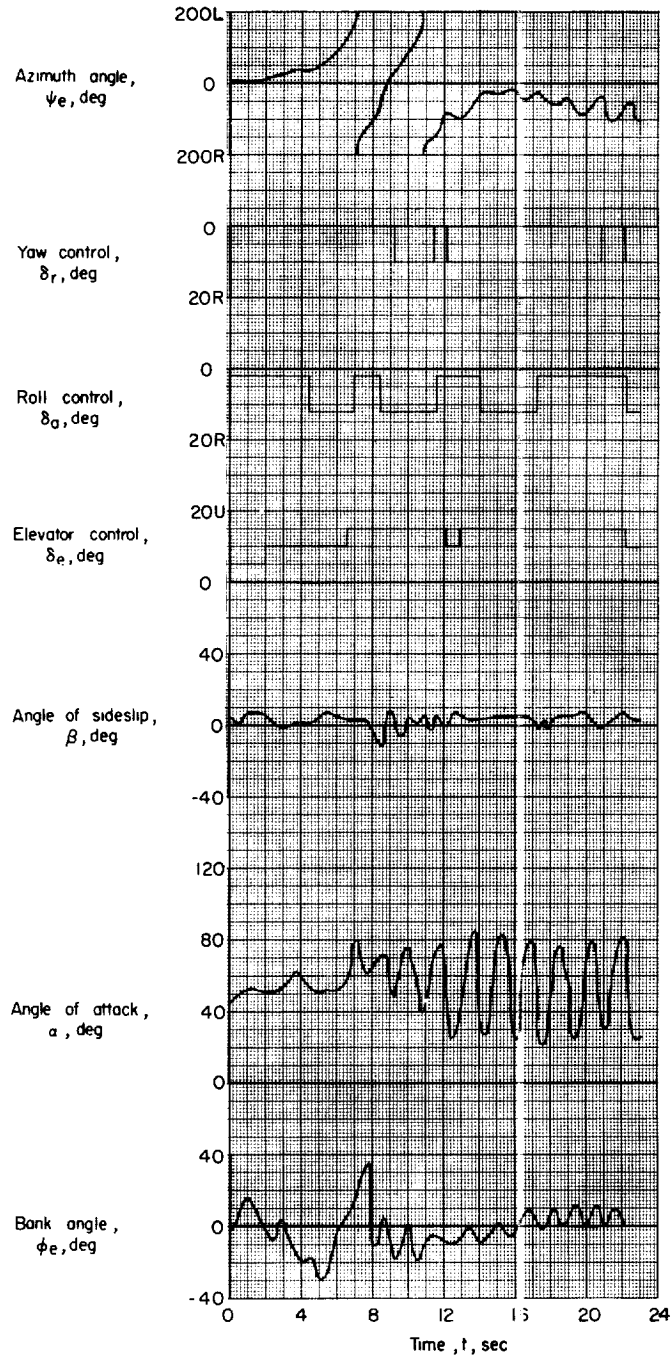
Figure 15.- Effect of variation of C_{l_p}, C_{n_p}, and C_{n_r} on the calculated damping of the Dutch roll oscillation.

L-1684

(a) $\delta_{e_{trim}} = -5^{\circ}$.

Figure 16.- Time history of typical flight tests with radio-controlled
model.

(b) $\delta_{e_{trim}} = -10°$.

Figure 16.- Concluded.